



Article

Photometric Catalogue for Space and Ground Night-Time Remote-Sensing Calibration: RGB Synthetic Photometry from *Gaia* DR3 Spectrophotometry

Josep Manel Carrasco^{1,2,3,*}, Nicolas Cardiel^{4,5}, Eduard Masana^{1,2,3}, Jaime Zamorano^{4,5}, Sergio Pascual^{4,5}, Alejandro Sánchez de Miguel^{4,5,6}, Rafael González⁴ and Jaime Izquierdo⁴

- ¹ Institut de Ciències del Cosmos (ICCUB), Universitat de Barcelona (IEEC-UB), Martí i Franquès 1, 08028 Barcelona, Spain; emasana@fqa.ub.edu
 - ² Departament de Física Quàntica i Astrofísica (FQA), Universitat de Barcelona (UB), Martí i Franquès 1, 08028 Barcelona, Spain
 - ³ Institut d'Estudis Espacials de Catalunya (IEEC), c. Gran Capità, 2-4, 08034 Barcelona, Spain
 - ⁴ Departamento de Física de la Tierra y Astrofísica, Facultad de CC. Físicas, Universidad Complutense de Madrid, Plaza de las Ciencias 1, 28040 Madrid, Spain; cardiel@ucm.es (N.C.); jzamorano@fis.ucm.es (J.M.); sergiopr@fis.ucm.es (S.P.); alejasan@ucm.es (A.S.d.M.); rafael08@ucm.es (R.G.); jiz@astrax.fis.ucm.es (J.I.)
 - ⁵ Instituto de Física de Partículas y del Cosmos, IPARCOS, Facultad de CC. Físicas, Universidad Complutense de Madrid, Plaza de las Ciencias 1, 28040 Madrid, Spain
 - ⁶ Environment and Sustainability Institute, University of Exeter, Penryn, Cornwall TR10 9FE, UK
- * Correspondence: carrasco@fqa.ub.edu



Citation: Carrasco, J.M.; Cardiel, N.; Masana, E.; Zamorano, J.; Pascual, S.; Sánchez de Miguel, A.; González, R.; Izquierdo, J. Photometric Catalogue for Space and Ground Night-Time Remote-Sensing Calibration: RGB Synthetic Photometry from *Gaia* DR3 Spectrophotometry. *Remote Sens.* **2023**, *1*, 0. <https://doi.org/>

Academic Editor: Firstname
Lastname

Received: 31 January 2023

Revised: 22 March 2023

Accepted:

Published:

Publisher's Note: MDPI stays neutral with regard to jurisdictional claims in published maps and institutional affiliations.



Copyright: © 2023 by the authors. Licensee MDPI, Basel, Switzerland. This article is an open access article distributed under the terms and conditions of the Creative Commons Attribution (CC BY) license (<https://creativecommons.org/licenses/by/4.0/>).

Abstract: Recent works have made strong efforts to produce standardised photometry in RGB bands. For this purpose, we carefully defined the transmissivity curves of RGB bands and defined a set of standard sources using the photometric information present in *Gaia* EDR3. This work aims not only to significantly increase the number and accuracy of RGB standards but also to provide, for the first time, reliable uncertainty estimates using the BP and RP spectrophotometry published in *Gaia* DR3 instead of their integrated photometry to predict RGB photometry. Furthermore, this method allows including calibrated sources regardless of how they are affected by extinction, which was a major shortcoming of previous work. The RGB photometry is synthesised from the *Gaia* BP and RP low-resolution spectra by directly using their set of coefficients multiplied with some basis functions provided in the *Gaia* catalogue for all sources published in *Gaia* DR3. The output synthetic magnitudes are compared with the previous catalogue of RGB standards available.

Keywords: ISS; light pollution; multispectral properties of lighting; calibration; GAIA; photometry

1. Introduction

RGB photometry has been increasingly used in recent decades for amateur and professional astronomical studies due to the high-quality and economically accessible digital cameras. In recent works [1,2], a strong effort was made to produce a standardised system for RGB photometry to enhance the quality of the studies to be performed with these kind of devices. This is relevant not only for ground measurements but also for satellite observations as stars are also being used to calibrate night-time remote-sensing platforms, such as the images taken from the International Space Station (ISS) [3] and the Suomi North Polar Partnership and NOAA-20, Visible Infrared Imaging Radiometer Suite Day Night Band (VIIRS) [4,5].

Ref. [1] defined the transmissivity passbands for RGB filters derived from 28 different types of cameras analysed by [6]. Ref. [1] also established standardised synthetic RGB photometry for

a set of 1346 bright stars belonging to the Bright Star Catalogue [7]. This small set of standards was expanded in number (about 15 million sources) by [2](hereafter, C21) using photometric transformations derived from integrated photometry in *Gaia* EDR3 [8,9]. This work aims to further expand the quality and number of sources in the sky with known RGB photometry that could be used as standards. For that purpose, we use synthetic photometry derived from the *Gaia* DR3 low-resolution spectra [10–12].

In *Gaia* DR3 [13], a set of 220 million sources were released together with their blue (BP) and red (RP) low-resolution spectra. When compared with RGB passbands (Figure 1), we can see that RGB passbands mostly cover only the wavelength range covered by BP instrument (In order to avoid confusion, specifically with the G band, in this paper, we used G_{Gaia} , G_{BP} and G_{RP} to refer to *Gaia* magnitudes and R_{RGB} , G_{RGB} and B_{RGB} for magnitudes in the RGB system.).

It is known [11,12,14] that the BP instrument has more calibration issues present than RP. Fortunately, most of these issues are assigned to difficulties in the ultraviolet region ($\lambda < 400$ nm), where the *Gaia* response decreases abruptly, and the amount of standards with enough flux in that range diminishes substantially. As none of the RGB passbands extends to so short wavelengths, we can still use *Gaia* spectrophotometry to derive synthetic RGB photometry from them.

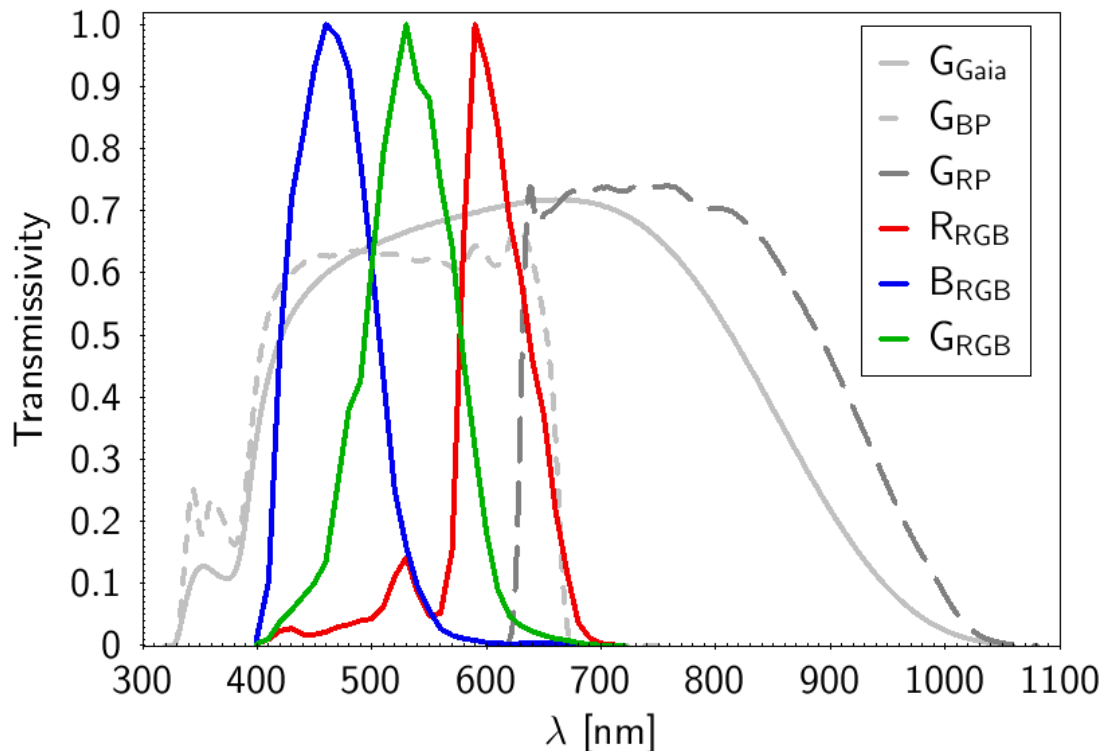


Figure 1. Comparison of RGB transmissivity curves (in colour lines) used in this work, extracted from [1] with the *Gaia* DR3 transmissivity curves by [9] (in grey). In order to distinguish between the G passband from the RGB system and the G passband from the *Gaia* system, we add 'RGB' as a subscript to the first and 'Gaia' as a subscript to the latter.

We describe, in Section 2, the methodology used to derive the synthetic photometry from *Gaia* spectrophotometry, producing the synthetic photometry for all sources with BP and RP spectra (hereafter, XP is used to refer to BP or RP spectra indistinctly) present in *Gaia* DR3 and not flagged as variable in the catalogue. In Section 3, we compare the samples of sources in this work with the ones used by C21, comparing also the RGB magnitudes obtained in both

studies. In Section 4, we study the validity of the polynomials defined in C21 for those sources in *Gaia* DR3 without XP spectra available. Section 5 explains how to access the final catalogue of RGB magnitudes created in this work (in form of an online table and through a Python code called RGBLOOM). Finally, we present a brief summary of the results and conclusions of this work in Section 6.

2. RGB Catalogue Construction

Gaia [15] is a survey mission, which allows homogeneously observing all sources in the sky up to magnitude 21. In addition to the 3D positions, motions and broad band photometry, *Gaia* also provides spectrophotometry for 219 million sources [10–12]. The astrophysical information contained in these spectra allows the study of the physical properties of the observed sources to analyse, for instance, their spectral features as performed in [16].

The homogeneity of the spectrophotometry over all sky positions also makes *Gaia* a suitable mission to be used as a reference to establish a catalogue of standard sources in any photometric system covering the optical range. This possibility to derive synthetic photometry from the *Gaia* spectrophotometry has been previously explored by several works [11,14,17,18]. We use here the same methodology (briefly described in the following paragraphs) to derive the synthetic photometry in RGB bands from XP *Gaia* DR3 spectrophotometry. Notice that, as recommended by [11], we do not use, in this work, the sampled spectra to derive the synthetic photometry; instead, we directly work with the source coefficients to obtain our estimations of the RGB magnitudes.

From the externally calibrated *Gaia* mean spectra, $f_s(\lambda)$, for a given source, s , we can derive its synthetic integrated flux (F_{sj}) in a given passband, j , with transmissivity equal to $T_j(\lambda)$ by deriving the following integral expression with wavelength λ :

$$F_{sj} = \frac{\int f_s(\lambda) \cdot T_j(\lambda) \cdot \lambda \, d\lambda}{\int T_j(\lambda) \cdot \left(\frac{c}{\lambda}\right) \, d\lambda}, \quad (1)$$

where the ABMAG system is considered for the zeropoint [19–21] with c as the speed of light.

The *Gaia* externally calibrated mean spectra $f_s(\lambda)$ is described as the weighted sum of the BP and RP contributions, $f_s^{\text{BP}}(\lambda)$ and $f_s^{\text{RP}}(\lambda)$, respectively:

$$f_s(\lambda) = w^{\text{BP}}(\lambda) \cdot f_s^{\text{BP}}(\lambda) + w^{\text{RP}}(\lambda) \cdot f_s^{\text{RP}}(\lambda), \quad (2)$$

with $w^{\text{BP}}(\lambda)$ and $w^{\text{RP}}(\lambda)$ as their weighted contributions to the total flux of each wavelength from the XP instruments.

In its turn, $f_s^{\text{BP}}(\lambda)$ and $f_s^{\text{RP}}(\lambda)$ are described as a set of N coefficients, b_{sn} , multiplied by a set of basis functions, φ_n :

$$f_s^{\text{XP}}(\lambda) = \sum_{n=1}^N b_{sn}^{\text{XP}} \cdot \varphi_n^{\text{XP}}(\lambda), \quad (3)$$

The set of basis functions, $\varphi_n^{\text{XP}}(\lambda)$, and weights, $w^{\text{XP}}(\lambda)$, were published together with *Gaia* DR3 and are available on this webpage: <https://www.cosmos.esa.int/web/gaia/dr3-xpmergexpsampling>, accessed on 12 July 2022.

Combining Equations (1)–(3), we can derive the synthetic flux, F_{sj} , in a given passband j as:

$$\begin{aligned} F_{sj} &= \sum_{n=1}^N b_{sn}^{\text{BP}} \cdot \left(\frac{\int w^{\text{BP}}(\lambda) \cdot \varphi_n^{\text{BP}}(\lambda) \cdot T_j(\lambda) \cdot \lambda \, d\lambda}{\int T_j(\lambda) \cdot \left(\frac{c}{\lambda}\right) \, d\lambda} \right) + \\ &+ \sum_{n=1}^N b_{sn}^{\text{RP}} \cdot \left(\frac{\int w^{\text{RP}}(\lambda) \cdot \varphi_n^{\text{RP}}(\lambda) \cdot T_j(\lambda) \cdot \lambda \, d\lambda}{\int T_j(\lambda) \cdot \left(\frac{c}{\lambda}\right) \, d\lambda} \right) \equiv \\ &\equiv \sum_{n=1}^N b_{sn}^{\text{BP}} \cdot X_{nj}^{\text{BP}} + \sum_{n=1}^N b_{sn}^{\text{RP}} \cdot X_{nj}^{\text{RP}}, \end{aligned} \quad (4)$$

where the X_{nj}^{XP} terms do not depend on the source and can be derived and stored previously for any passbands and then applied to any required source using their b_{sn}^{XP} coefficients without the need to recompute X_n^{XP} terms again.

These integrated fluxes can be also expressed in terms of ABMAG system magnitudes, m_{sj} , by using the flux in that passband measured for an input flux of $3.631 \times 10^{-23} \text{ W/Hz/m}^2$. We name that flux as ZP_j . Thus, the magnitude can be expressed as:

$$m_{sj} = -2.5 \log \left(\frac{F_{sj}}{ZP_j} \right). \quad (5)$$

From the covariance matrix, C_{nm}^{XP} , assigned to the source coefficients, we can also derive the uncertainty in the derived magnitudes as:

$$\sigma_{sj} = \sqrt{A_j^{\text{BP}} + A_j^{\text{RP}}}, \quad (6)$$

where A_j^{XP} can be derived using:

$$A_j^{\text{XP}} = \sum_{n=1}^N X_{nj}^{\text{XP}} \cdot \left(\sum_{m=1}^N C_{nm}^{\text{XP}} \cdot X_{mj}^{\text{XP}} \right). \quad (7)$$

Gaia DR3 published a total of 219,197,643 sources (see De Angeli et al. [11]) with XP continuous spectra. From these, a total of 6,093,025 sources have the flag `phot_variable_flag = 'VARIABLE'`. We show the variable sources subtracted from the sample in colour-magnitude diagrams (Figure 2) as well as their G_{Gaia} and $G_{\text{BP}} - G_{\text{RP}}$ histograms (Figure 3).

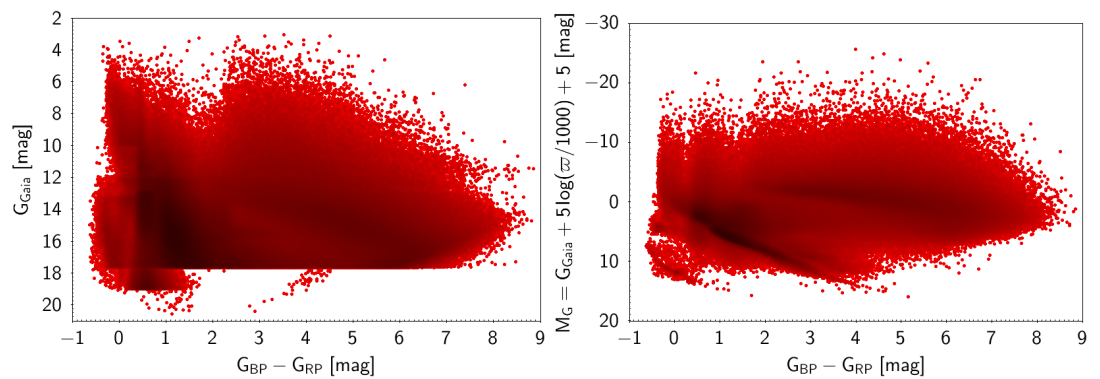


Figure 2. Magnitude-colour diagrams for sources with `phot_variable_flag='VARIABLE'` (excluded from our study) with continuous XP spectra in *Gaia* DR3 using the apparent (left) and absolute (right) magnitude.

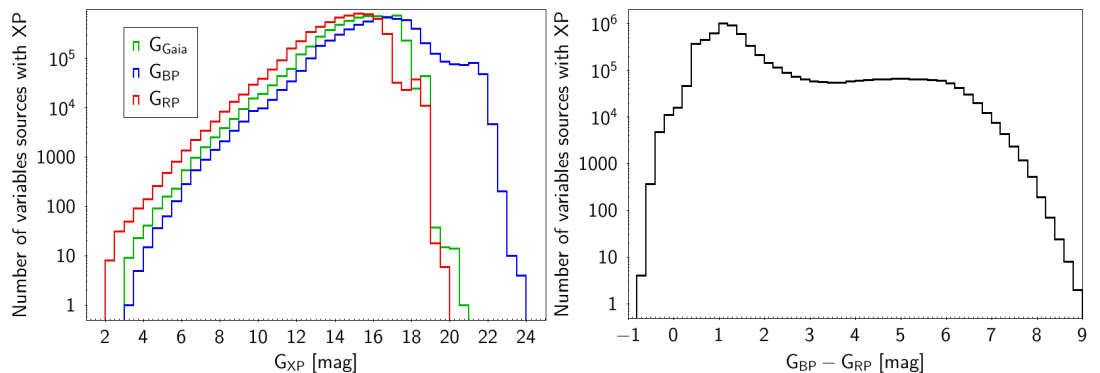


Figure 3. G_{Gaia} magnitude (left) and $G_{\text{BP}} - G_{\text{RP}}$ (right) histograms for sources with `phot_variable_flag='VARIABLE'` (excluded from our study) with continuous XP spectra in *Gaia* DR3.

These variable sources cannot be considered here for our purposes of establishing a set of reliable RGB standards. We also aimed to select only sources with `phot_variable_flag='CONSTANT'`; however, no sources with *Gaia* DR3 XP spectra have this flag value, as only sources with `phot_variable_flag='NOT_AVAILABLE'` and `'VARIABLE'` are present in the catalogue. This is because *Gaia* DR3 is still an intermediate release and because the mission has not yet finished to be completely sure that a given source is really constant. Future *Gaia* releases could identify some sources finally included in the catalogue as variables when considering a larger time interval covering the full mission. Although other types of sources (quasars, galaxies, crowded fields, etc.) were not suitable to be used as RGB standards, we decided to keep them in the catalogue in order to allow a wider range of applications for this catalogue, and only explicit variable sources identified by the *Gaia* catalogue were excluded from it. With the large density of sources available in the new catalogue, a posterior outlier identification, based on statistical analysis, can be conducted in order to exclude them from the calibration procedure.

Thus, we derived the RGB synthetic magnitudes for all 213,104,618 sources with `phot_variable_flag != 'VARIABLE'`. After removing 40,616 sources with unreliable RGB magnitude estimates, a final sample of 213,064,002 objects was created—hereafter, the 200 M sample. In a small subsample of this collection, the RGB magnitude estimates are missing in some of the 3 bands (159,456, 14,546 and 486 objects in B_{RGB} , G_{RGB} and R_{RGB} , respectively). This is likely due to very low signal in these wavelength ranges present in the *Gaia* spectrophotometry. We decided to keep the affected sources because, in all these cases, a magnitude estimate is available in at least one of the RGB bands.

As the number of variable sources represents less than 3% of the total number of *Gaia* DR3 sources with XP data, the general plots included in [11] to describe *Gaia* DR3 XP data, can also be used here to describe the main characteristics of our catalogue of RGB standards. The only missing sources in our sample are the ones represented in Figures 2 and 3.

3. Comparison with the C21 Sample

The new 200 M sample exhibits clear advantages over its predecessor published by C21. The most obvious advantage is the fact that the RGB magnitude estimates are directly computed from the source spectrum without the need to employ any approximate calibration, nor introducing constraints on the source colour or extinction. In this section, we provide a more detailed description of the benefits of using the new 200 M sample provided with this paper.

3.1. Number of Calibrated Sources

With this work, we move from the ~ 15 million sources in C21 to more than 200 million objects. This can be easily visualized in the maps displayed in Figure 4, which represent the density of sources on the celestial sphere in Galactic coordinates (using a Mollweide projection with HEALPIX of level 6 with a pixel size of 0.84 square degrees). Not surprisingly, the 200 M sample is concentrated towards the Galactic plane, not being affected by the scarcity of sources in the directions of high interstellar extinction as seen with the C21 sample.

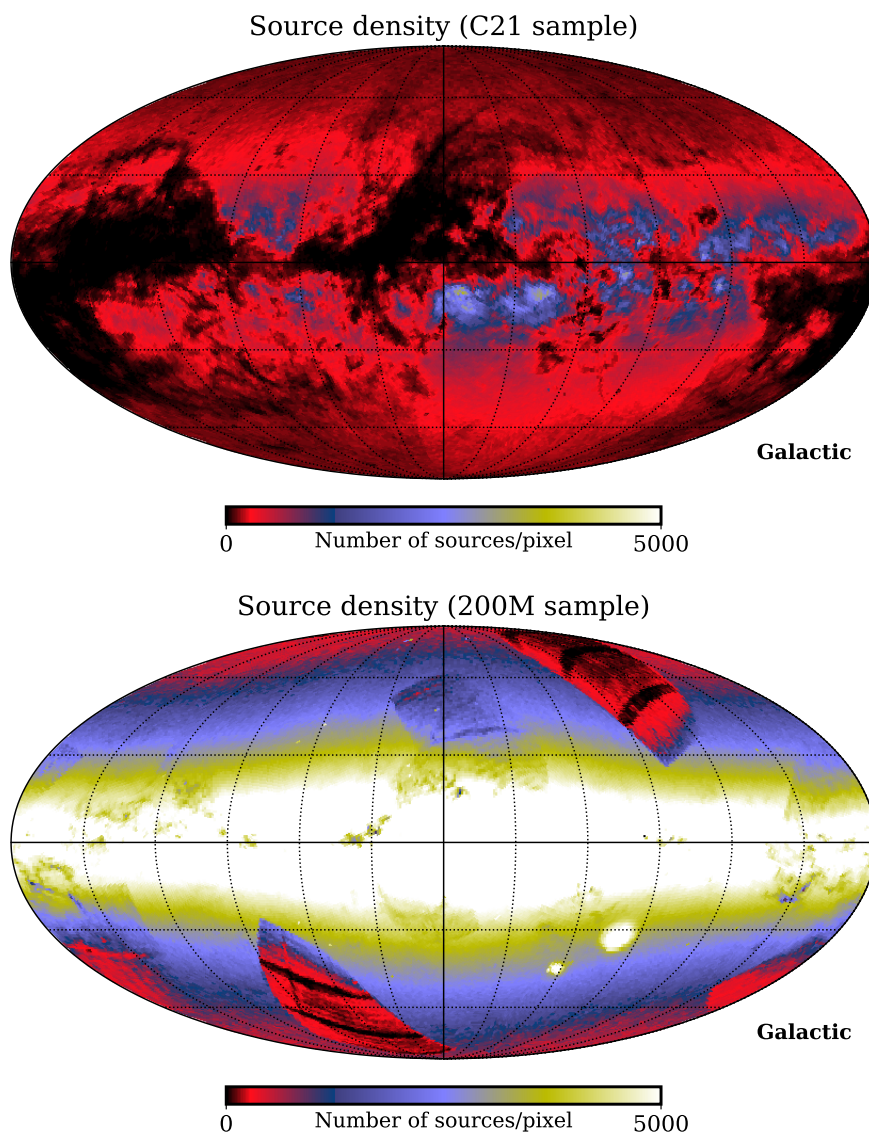


Figure 4. Source density maps, in Galactic coordinates, corresponding to the C21 (**top**) and the 200 M (**bottom**) samples. These maps were created using HEALPIX of level 6 (providing a pixel size of 0.84 square degrees) and are colour coded depending on the number of sources within the pixel. Note that the colour scale is the same in both maps. See Figure 5 for a histogram comparison of the source density in these maps.

The corresponding histograms of the source density are displayed in Figure 5. Panel (a) shows that, as expected, there are many directions in the celestial sphere in which the density of stars corresponding to the 200 M sample is clearly larger than as shown by the sources in the C21 sample. The zoom near the origin, panel (b), reveals that the density distribution of the C21 sample is bimodal with a first peak in the first histogram bin, corresponding to the interval $[0, 10]$ objects/pixel and a second peak in the interval $[120, 130]$ objects/pixel. The first peak corresponds to the directions of high extinction that are purposely excluded by C21.

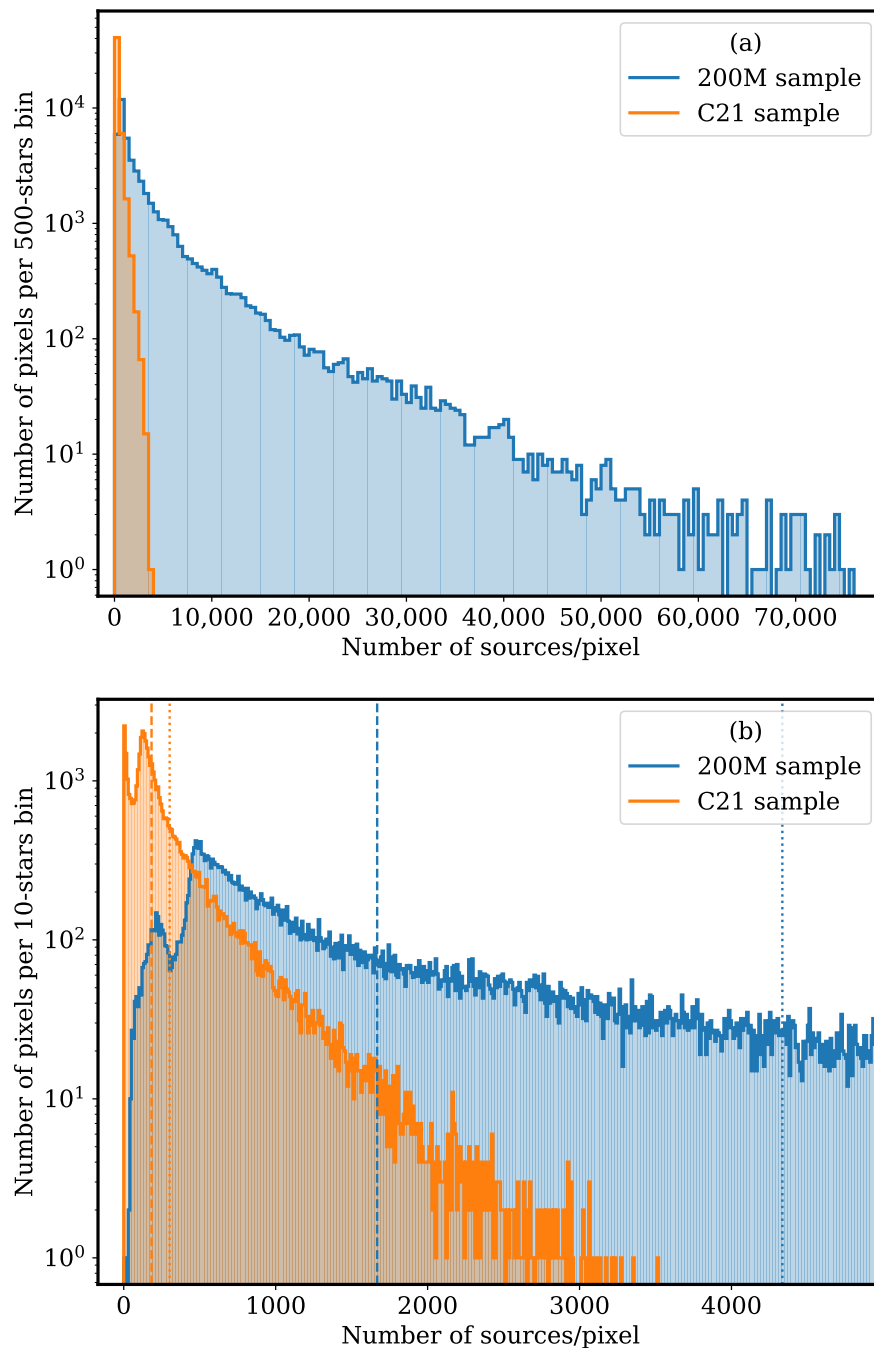


Figure 5. Panel (a): histograms of the source density (i.e., number of sources/pixel, where each pixel corresponds to 0.84 square degrees) in the maps displayed in Figure 4 for the 200 M sample (blue) and for the C21 sample (orange). Panel (b): zoom of the previous plot near the origin. The vertical lines indicate the mean values (302 and 4335 objects/pixel for C21 and 200 M, respectively; dotted lines) and median values (183 and 1668 objects/pixel for C21 and 200 M; dashed lines) for each sample. Note that a different bin size is employed in each panel as indicated in the label of the vertical axis.

The 200 M histogram is also bimodal with a first peak in the interval [210, 240] objects/pixel and a higher second peak in the interval [470, 480] sources/pixel. This reflects the selection criteria chosen to publish XP spectra for *Gaia* DR3 (see De Angeli et al. [11]). In both

samples, the histogram distributions are clearly asymmetric as indicated by the location of their respective means (vertical dotted lines) and medians (vertical dashed lines), whose values are given in the figure caption.

Considering that the pixel size employed in the maps displayed in Figure 4 is slightly below 1 square degree, we confirm that the 200 M sample offers several hundred sources per square degree in most regions of the sky. A more detailed calculation indicates that 99.7% of the celestial sphere is covered with a source density above 100 sources/(square degree) by this catalogue. The rest of the sky with less sources present corresponds to regions in the *Gaia* mission with less transits and without *Gaia* spectrophotometry available in *Gaia* DR3 [11].

Clearly, the above numbers should be taken with some caution because, in a practical way, the number of usable sources will also be a function of the magnitude limit reached. In this sense, Figure 6 displays the variation in the number of sources as a function of the magnitude in the G_{RGB} band. The plot shows the histogram (dotted lines) and the cumulative sum (thick full lines) for the C21 (orange) and the 200 M samples (blue). In both samples, there is a sudden decrease in the number of sources for $G_{\text{RGB}} \gtrsim 17.5$ mag.

This is because most of the sources published in *Gaia* DR3 were selected to have $G_{\text{Gaia}} < 17.65$ mag, although the XP spectra for some sources (including white dwarfs, galaxies and quasars) were also explicitly published above this magnitude limit (see De Angeli et al. [11]). The cumulative number of stars down to some particular G_{RGB} values are listed in Table 1. The M200 sample clearly outnumbers the C21 sample in number of sources at any magnitude value.

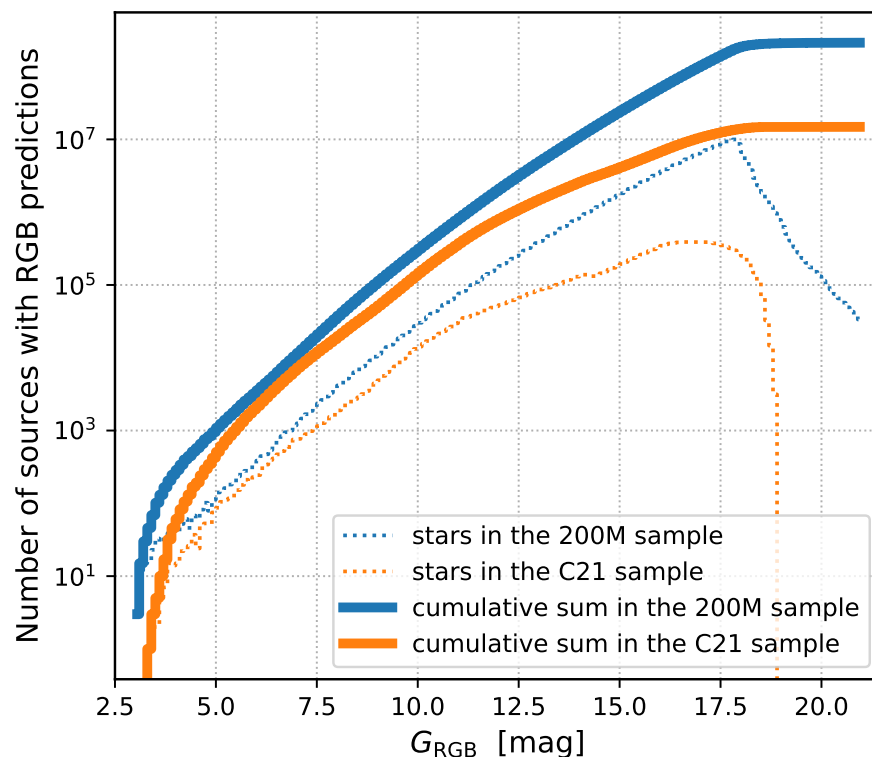


Figure 6. Variation in the number of sources with RGB magnitude predictions as a function of G_{RGB} for both the 200 M (blue) and the C21 (orange) samples. The dotted lines show the histograms in bins of 0.1 mag, whereas the thick full lines display the cumulative sums.

Table 1. Cumulative sums down to some particular G_{RGB} value for the C21 and the 200 M samples.

G_{RGB} Interval [mag]	Sources in C21	Sources in 200 M
<10	133,019	299,041
<11	344,349	775,526
<12	761,279	1,948,176
<13	1,431,314	4,636,535
<14	2,484,448	10,495,506
<15	3,977,325	22,967,532
<16	6,546,925	48,355,681
<17	10,346,030	97,464,183
<18	13,820,929	182,081,668
<19	14,854,959	209,094,405
<20	14,854,959	212,129,751
$\lesssim 21$	14,854,959	213,064,002

3.2. Source Characteristics

Apart from the different number of sources included in the 200 M and C21 samples, important differences in some specific characteristics of the sources are worth mentioning. In particular, the C21 subsample was restricted to sources with $-0.5 \leq G_{\text{BP}} - G_{\text{RP}} \leq 2.0$ mag, whereas the 200 M sample does not include this constraint. This is clearly manifested in the histogram displayed in Figure 7, which shows that the new 200 M sample (blue filled histogram) also includes much redder objects that were not included in the C21 sample (black line).

In addition, this figure also represents the histograms corresponding to the 200 M subsamples corresponding to particular sources not classified as simple stars in *Gaia* DR3 (namely the sources flagged as `non_single_star`, `in_qso_candidates` and `in_galaxy_candidates`), for which the polynomial RGB calibration in C21, derived only for single stars, is not suitable.

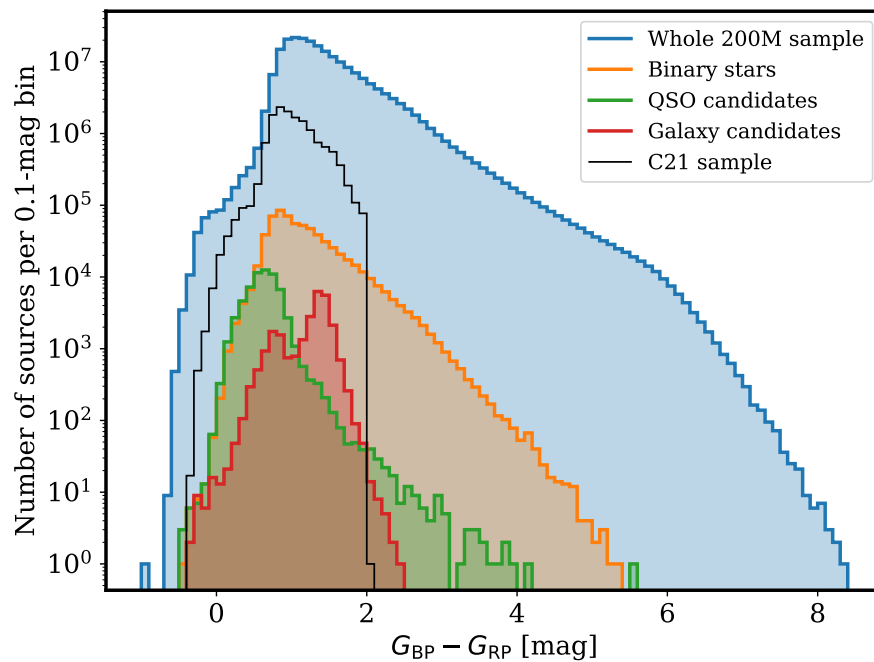


Figure 7. Histogram of the 200 M sample as a function of $G_{BP} - G_{RP}$ colour in bins of 0.1 mag. The whole 200 M sample is displayed in blue, whereas the subsamples corresponding to sources flagged in *Gaia* DR3 as `non_single_star`, `in_qso_candidates` and `in_galaxy_candidates` are displayed in orange, green and red, respectively. In addition, the histogram corresponding to the C21 sample is displayed with a thin black line, which is limited to $-0.5 \leq G_{BP} - G_{RP} \leq 2.0$ mag.

We also explore, in Figure 8, the histogram distribution of some additional parameters derived from the *Gaia* DR3 data, in particular, the `distance_gspphot` (in kpc, panel (a)) and extinction in the G_{Gaia} band `ag_gspphot` (in magnitudes, panel (b)) as well as typical stellar parameters, such as the effective temperature `teff_gspphot` (in K, panel (c)), surface gravity `logg_gspphot` (logarithm of cgs units, panel (d)) and global metallicity `mh_gspphot` (dex units, panel (e)). The 200 M sample contains proportionally more distant sources than does the C21 sample, although the most noticeable difference is the inclusion of more sources with much larger extinction. The 200 M catalogue incorporates proportionally more stars with large effective temperature, low surface gravity and low metallicity.

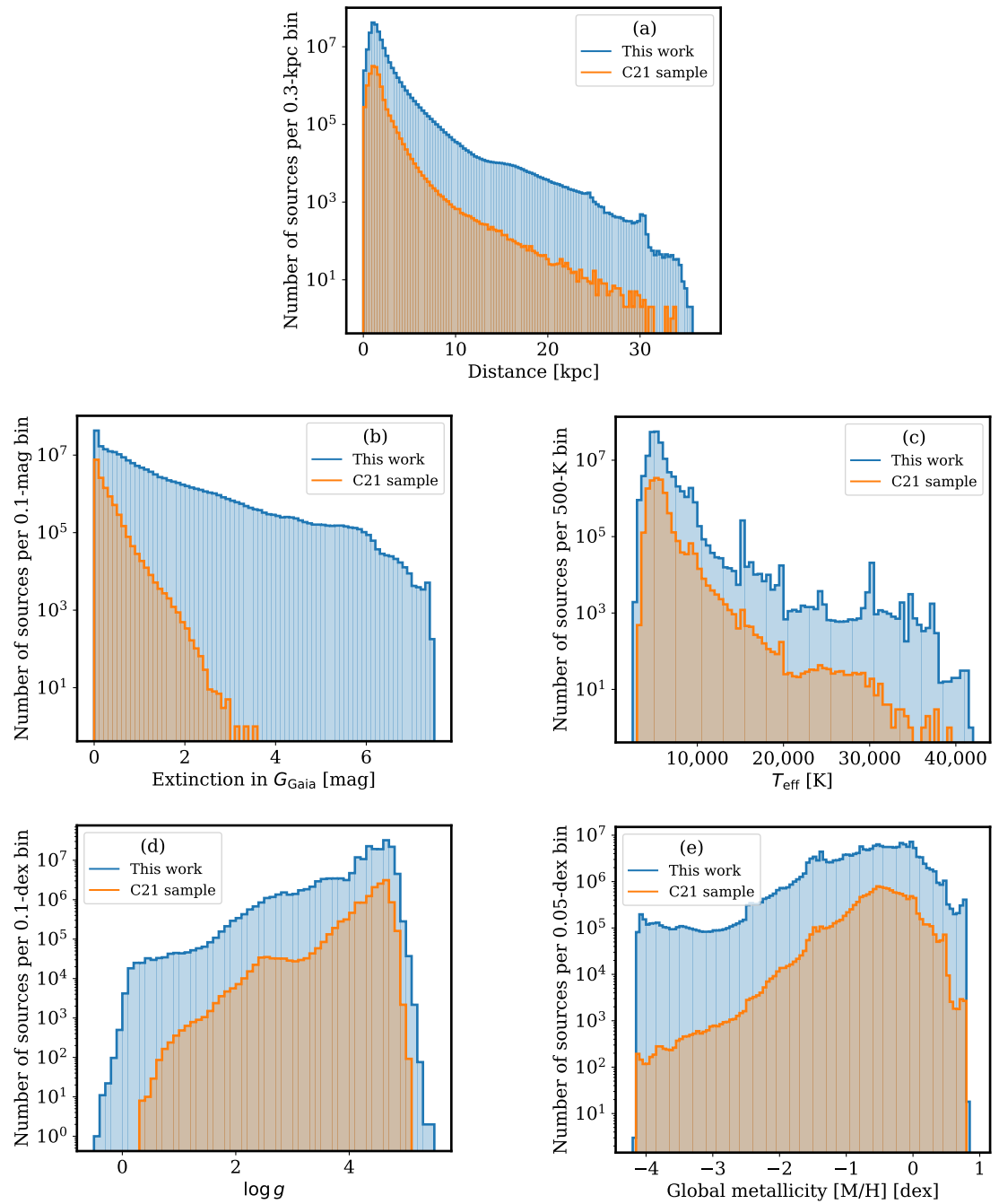


Figure 8. Comparison between the 200 M sample built in this work (blue histograms) and the C21 sample (orange histograms). The panels represent different parameters retrieved from the *Gaia* DR3 database, namely distance_gspphot (in kpc, panel (a)) and extinction in the G_{Gaia} band ag_gspphot (in magnitudes, panel (b)) as well as typical stellar parameters, such as the effective temperature $t_{\text{eff_gspphot}}$ (in K, panel (c)), surface gravity $\log g_{\text{gspphot}}$ (logarithm of cgs units, panel (d)) and global metallicity $m_{\text{h_gspphot}}$ (dex units, panel (e)).

3.3. Magnitude Residuals

As the synthetic photometry in the 200 M sample is derived directly from the observed spectra and not predicted based on broad band photometry, the values obtained in this work

should be more accurate than those provided by C21. Thus, the level of discrepancy should be mainly constrained by the precision of C21. We compare, in Figures 9 and 10, the synthetic photometry derived here with the predictions provided by C21 for 12,920,293 non-variable sources in common. As expected, the discrepancies mostly fall in the ± 0.1 mag range, which was the required accuracy claimed in C21. This provides confidence in the validity of our results.

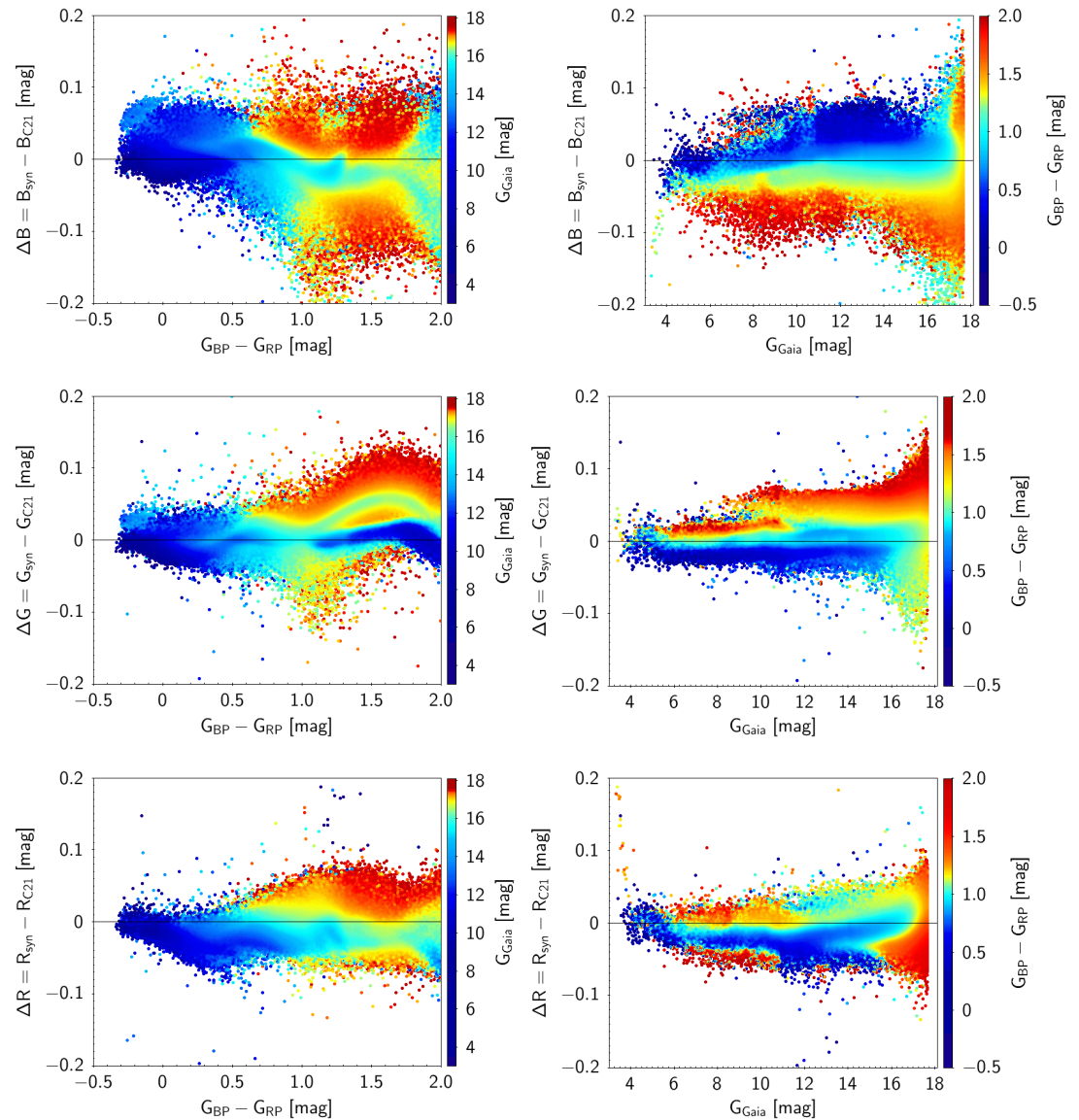


Figure 9. Difference between the synthetic magnitude computed in this work (X_{syn}) and those provided by C21 (X_{C21}) for $X = B_{\text{RGB}}$ (top row), G_{RGB} (middle row) and R_{RGB} (bottom row) as a function of *Gaia* $G_{\text{BP}} - G_{\text{RP}}$ colour (left column) and G_{Gaia} magnitude (right column) for non-variable sources in common.

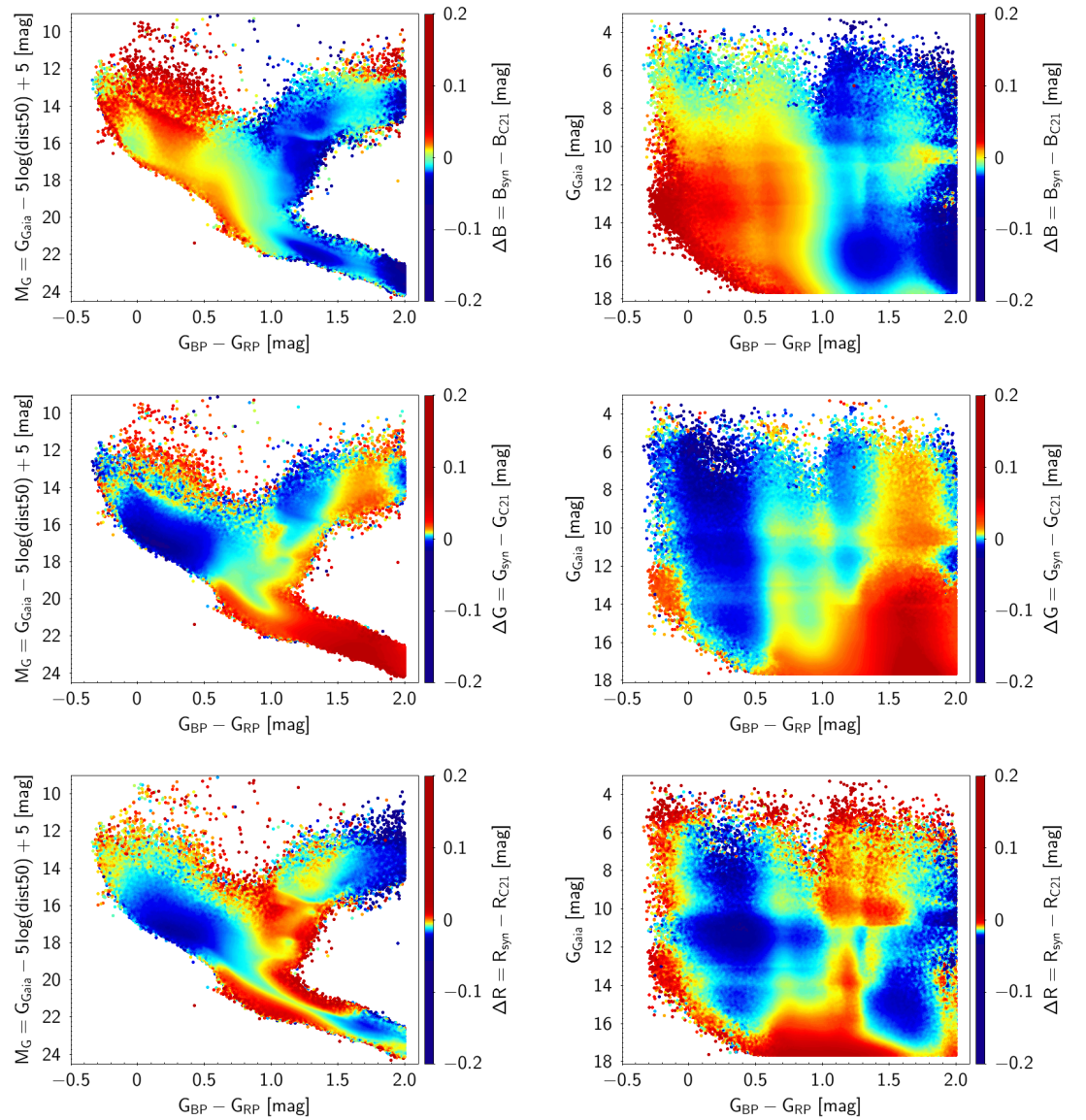


Figure 10. Absolute (left column) and apparent (right column) *Gaia* magnitude-colour diagrams for non-variable sources in common with C21. The colour index shows the difference between the synthetic magnitude (X_{syn}) and those provided by C21 (X_{C21}) for $X = B_{\text{RGB}}$ (top row), G_{RGB} (middle row) and R_{RGB} (bottom row).

The observed biases and colour trends in the differences shown in Figures 9 and 10 are due to systematics in the *Gaia* spectra (see *Gaia* Collaboration et al. [14]) and the photometric transformations proposed by C21—being more important for the latter. The ‘bridge’ structure present in the G_{RGB} residual (middle-left panel in Figure 9) with $1.0 < G_{\text{BP}} - G_{\text{RP}} < 2.0$ mag contains main sequence stars, although giants have lower levels of residuals).

On the other hand, the results in the right panels of Figures 9 and 10 show the different behaviour present for $G_{\text{Gaia}} < 11.5$ mag with respect to fainter magnitudes. This feature is likely induced by *Gaia* XP data as sources with $G_{\text{Gaia}} < 11.5$ mag are observed with different gating strategies in *Gaia* to avoid saturation (see [15,22]). For these bright *Gaia* sources, larger systematics are expected in the XP spectra due to the lower number of calibrators present for those special gating conditions used to minimise saturation events in *Gaia*.

The method for deriving the synthetic RGB magnitudes explained in Section 2 allows for the derivation of the associated uncertainties, and it is possible to examine their behaviour as a function of the relevant parameters. In particular, Figure 11 represents 2D histograms with the density of sources as a function of G_{Gaia} (the horizontal axis) and the uncertainties in the synthetic magnitudes B_{RGB} , G_{RGB} and R_{RGB} (panels (a), (b) and (c), respectively). Not surprisingly, the uncertainties increase when moving to fainter objects. The red filled circles mark the 99th percentile at each 0.4 mag bin in the horizontal axis. Interestingly, these numbers are below 0.01 mag for a wide G_{Gaia} interval, increasing beyond $G_{\text{Gaia}} \gtrsim 14$ mag.

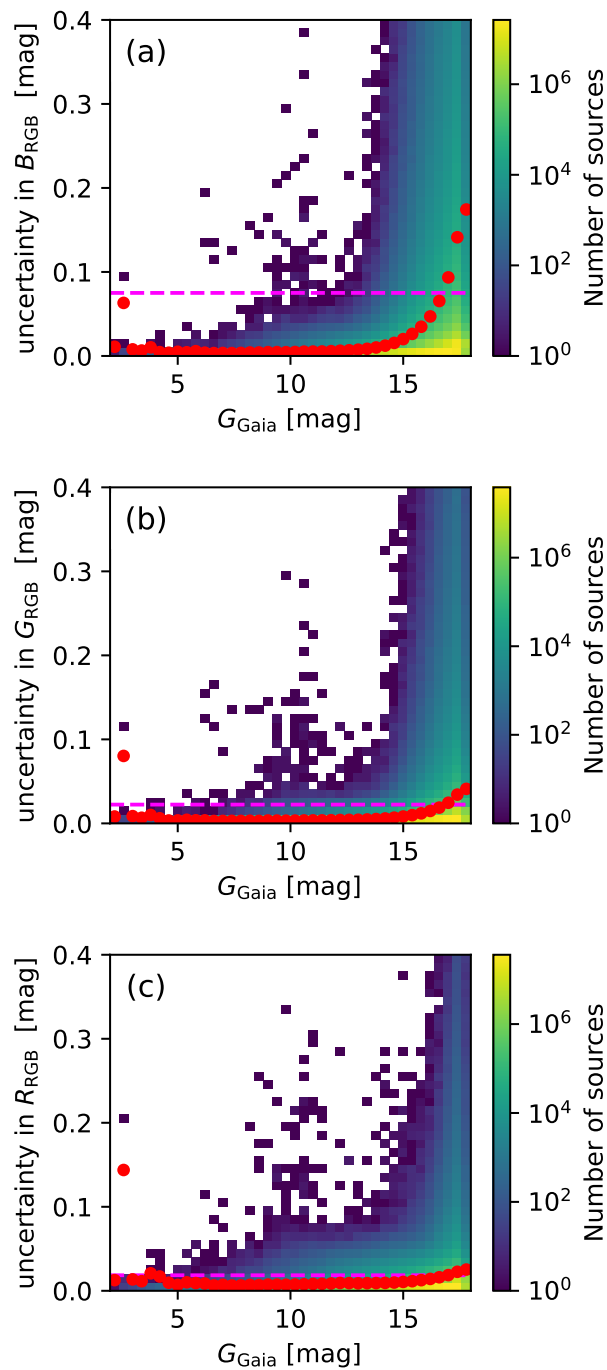


Figure 11. 2D histograms showing the number of sources as a function of G_{Gaia} (the horizontal axis; using 0.4 mag bins) and the uncertainties in the synthetic B_{RGB} (panel (a)), G_{RGB} (panel (b)) and R_{RGB} (panel (c)) magnitudes (vertical axis; using 0.01 mag bins), computed as explained in Section 2. The red filled circles indicate the 99th percentile at each bin in the horizontal axis, which reveals that, for most G_{Gaia} bins, these numbers are below 0.01 mag in the vertical axis with the exception of one bin at the bright extreme, $2.4 \leq G_{\text{Gaia}} \leq 2.8$ mag and for the fainter sources beyond $G_{\text{Gaia}} \gtrsim 14$ mag. The magenta dashed horizontal line indicates the 99th percentile for the whole sample with values of 0.075, 0.022 and 0.019 mag for B_{RGB} , G_{RGB} and R_{RGB} , respectively.

Since the number of faint sources is larger than the number of bright ones, the 99th percentiles for the whole sample with values of 0.075, 0.022 and 0.019 mag for B_{RGB} , G_{RGB} and R_{RGB} , respectively, (represented with the dashed horizontal magenta line in each panel) are naturally larger than the values for bright sources (with lower uncertainties but less abundant in the total sample). It is important to highlight that, although the uncertainties are unavoidably larger for fainter objects, the also larger number of available sources at those magnitude regimes should allow the simultaneous observation of many more of them to be used as standards. The statistical combination of these measurements should help to diminish the uncertainties at the faint end.

4. Validity of the C21 Polynomial Calibration

Considering that the 200 million of sources with XP spectra in *Gaia* DR3 represents only 10% of the total two billion sources with available *Gaia* photometry, we explore here the validity of the polynomial calibrations published by C21 to estimate RGB magnitudes for the missing sources. With this aim, we applied those polynomial functions to the 200 M subsample verifying $-0.5 \leq G_{\text{BP}} - G_{\text{RP}} \leq 2.0$ mag (the same constraint employed by C21) and derived the differences with the RGB estimates derived from the synthetic photometry computed in this work. The histograms of those differences are represented in Figure 12 for the B_{RGB} , G_{RGB} and R_{RGB} bands (panels (a), (b) and (c), respectively).

Each panel represents the histogram corresponding to the full subsample after applying the colour constraint (~ 182 million objects—hereafter, 182M samples; blue filled histogram) as well as the histograms of those sources that are not classified as single stars (with the same criteria employed in Figure 7). Interestingly, 93.6%, 97.8% and 98.3% of the sources exhibit differences within the ± 0.1 mag interval for B_{RGB} , G_{RGB} and R_{RGB} , respectively, (note that the vertical scale in the histograms is logarithmic). It is also evident that RGB predictions for objects flagged as *in_qso_candidates* and *in_galaxy_candidates* exhibit much larger deviations, although they have a small contribution in the total number of sources.

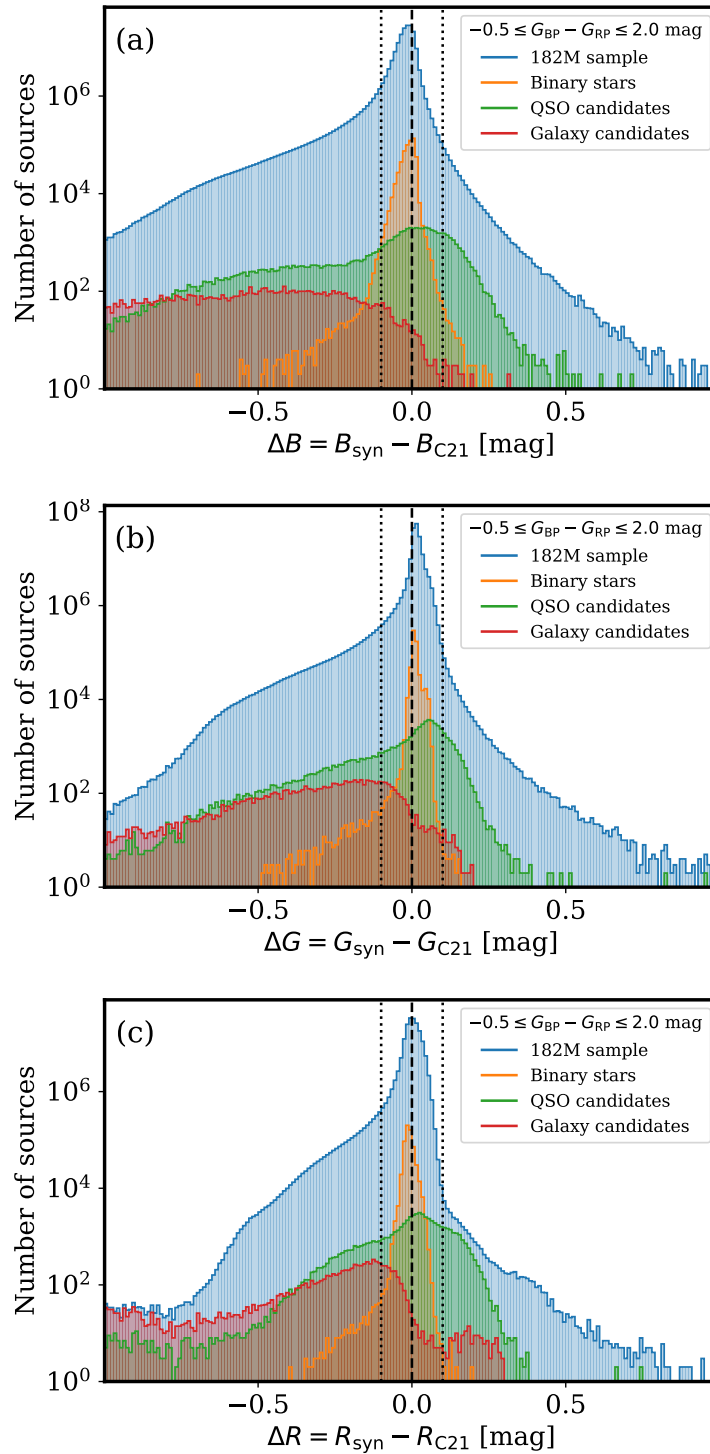


Figure 12. Histograms displaying the differences in the prediction of RGB magnitudes between the values derived in this work from the *Gaia* XP low-resolution spectra and those estimated using the polynomial functions published by C21. Since the latter are valid only for $-0.5 \leq G_{BP} - G_{RP} \leq 2.0$ mag, we applied here the same constraint to the 200 M sample (as indicated in the legend title), which reduces, in this analysis, the 200 M sample to ~ 182 million objects (182 M sample). Panels (a), (b) and (c) show the results for the B_{RGB} , G_{RGB} and R_{RGB} bands, respectively. Within each panel, we segregate the resulting histograms as shown in Figure 7. The vertical dashed line corresponds to $\Delta X = X_{syn} - X_{C21} = 0$ mag with $X = B_{RGB}$, G_{RGB} and R_{RGB} , whereas the vertical dotted lines are used in each panel to highlight the ± 0.1 mag interval, which encompasses 93.6%, 97.8% and 98.3% of the sources in panels (a), (b) and (c), respectively. 2D histograms representing the same dataset as a function of relevant parameters are shown in Figure 13.

An expanded representation of the above results is shown in the 2D histograms displayed in Figure 13, where the magnitude differences are represented as a function of G_{Gaia} with colour coding for the histograms according to the source density (first column, panels (a), (b) and (c)), extinction in G_{Gaia} (second column, panels (d), (e) and (f)) and $G_{\text{BP}} - G_{\text{RP}}$ (third column, panels (g), (h) and (i)). These histograms reveal a systematic offset for very bright sources (saturated in *Gaia* XP spectra; see Riello et al. [9] and De Angeli et al. [11]).

The figure also shows an expected increase in the differences of the magnitude predictions when considering fainter objects. Interstellar extinction has an important impact on the derived residuals, specifically in panels (d) and (e) for sources with $G_{\text{Gaia}} > 13$ mag. There are also some clear systematic magnitude differences depending on the source $G_{\text{BP}} - G_{\text{RP}}$ colour. Notwithstanding these relevant differences in the prediction of RGB magnitudes when using the C21 polynomial functions, it is important to highlight that, as previously mentioned, the predictions still fall within the ± 0.1 mag interval for a large fraction of the considered sources.

Thus, although the 200 M sample provides more reliable RGB predictions, the C21 calibrations may still be useful when used with the corresponding caution (i.e., avoiding high extinction regions, restricting the $G_{\text{BP}} - G_{\text{RP}}$ source colour and using a large number of calibrating sources in order to derive statistical averages).

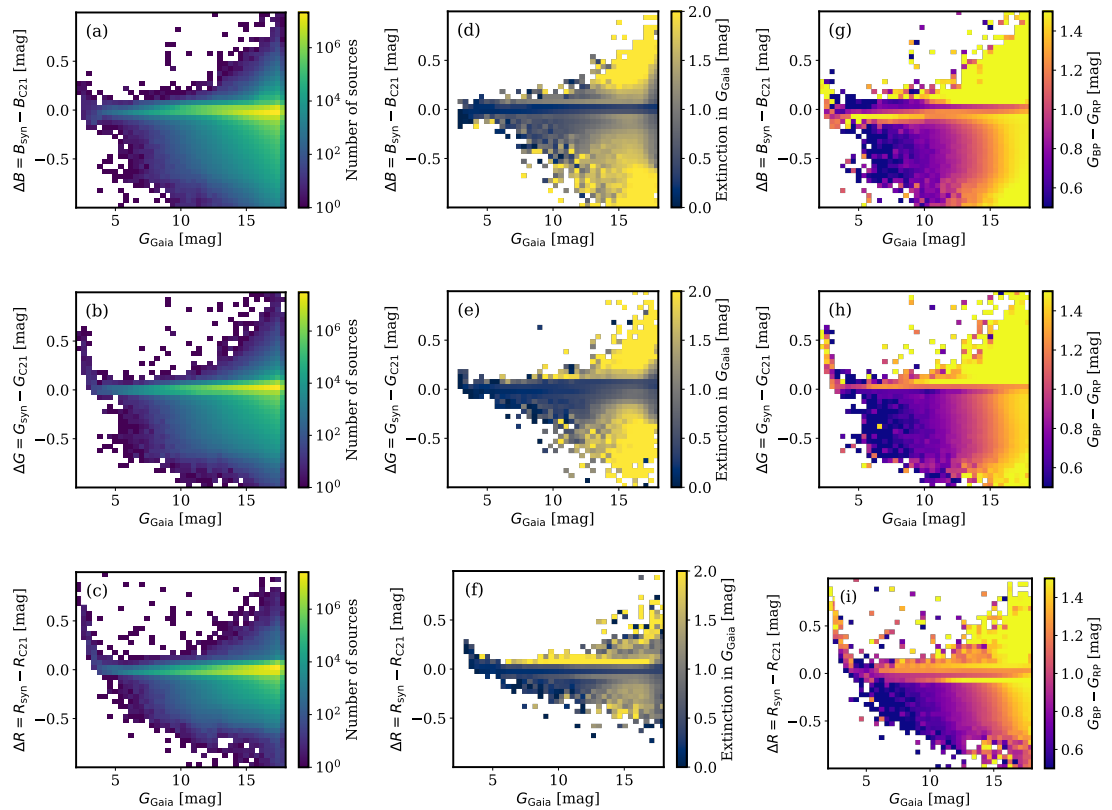


Figure 13. 2D histograms representing the number of sources (left column, panels (a–c)), the extinction in G_{Gaia} (middle column, panels (d–f)) and the colour $G_{\text{BP}} - G_{\text{RP}}$ (right column, panels (g–i)) as a function of G_{Gaia} (the horizontal axis; using 0.4 mag bins) and $\Delta X = X_{\text{syn}} - X_{\text{C21}} = 0$ mag with $X = B_{\text{RGB}}, G_{\text{RGB}}$ and R_{RGB} (the vertical axis; employing 0.05 mag bins). Each row displays the results for the $B_{\text{RGB}}, G_{\text{RGB}}$ and R_{RGB} bands (from top to bottom, respectively). These plots are an expanded version of the blue histograms shown in Figure 12, i.e., we are using the subset of the 200 M sample verifying $-0.5 \leq G_{\text{BP}} - G_{\text{RP}} \leq 2.0$ mag.

5. Accessing the 200 M Sample

The 200 M sample produced in this work is accessible through an online table (Table 2 shows the first rows of the catalogue), which is available as a large, (5.0 GB) single, compressed CSV file (available at https://nartex.fis.ucm.es/~ncl/rgbphot/gaiaDR3/RGBsynthetic_NOVARIABLES_sortida_XpContinuousMeanSpectrum_RGB_NOVARIABLES_final.csv.gz, accessed on 24 March 2023) (15 GB after decompressing). The flag −99.0 is employed in this table to indicate missing values in any of the RGB magnitudes or in their associated uncertainties.

As mentioned in Section 2, we have not removed the small fraction of objects in the 200 M sample classified in *Gaia* DR3 as belonging to one of the following categories: *non_single_star* (0.31% of the sample), *in_qso_candidates* (0.03%) and *in_galaxy_candidates* (0.01%). Although none of them have been thus far identified as a variable by *Gaia*, their use as reliable RGB calibrators should be properly checked through the statistical comparison with reliable sources located in their neighbourhood. All these sources are identified with the flag *objtype* in Table 2.

Table 2. First rows of the online table with the synthetic RGB magnitudes (B_{RGB} , G_{RGB} and R_{RGB}) and their associated uncertainties (σ_B , σ_G and σ_R) derived for the 200 M sample from the *Gaia* DR3 XP spectra for non-variable sources in the *Gaia* catalogue with id number equal to *source_id*. The column *objtype* is a flag that indicates the type of object in *Gaia* DR3: 1 for sources flagged as *non_single_star*, 2 for objects in *in_qso_candidates*, 3 for sources in *in_galaxy_candidates* and 0 for the rest of the sample. In addition, the last column, *qlflag*, provides a global quality flag, which is 0 for reliable sources and 1 for objects with any indication of potential problem (blending, contamination or non-stellar identification). The full table can be downloaded from the link provided in the text, and will also be available at the CDS.

<i>source_id</i>	B_{RGB}	G_{RGB}	R_{RGB}	σ_B	σ_G	σ_R	<i>objtype</i>	<i>qlflag</i>
4295806720	18.245	17.935	17.678	0.011	0.009	0.011	0	0
38655544960	15.003	14.570	14.171	0.003	0.002	0.002	0	0
1275606125952	16.849	16.519	16.266	0.005	0.004	0.006	0	0
1653563247744	16.544	16.336	16.196	0.005	0.004	0.005	0	0
2851858288640	12.779	12.550	12.387	0.001	0.001	0.002	0	0
3332894779520	13.335	12.894	12.539	0.002	0.001	0.002	0	0
3371550165888	15.314	14.938	14.615	0.003	0.002	0.003	0	1
3508989119232	15.736	15.431	15.199	0.003	0.003	0.003	0	0
4711579935744	14.736	14.481	14.300	0.002	0.002	0.003	0	0
4814659150336	18.490	17.854	17.297	0.013	0.009	0.009	0	1
5192616270720	18.370	17.551	16.964	0.013	0.007	0.007	0	0
5291399870976	17.301	17.033	16.842	0.006	0.005	0.007	0	0
5291399871488	18.935	18.296	17.686	0.019	0.012	0.011	0	0
.
.
.

In addition, we also assigned a global quality flag to each source, *qlflag*, provided in the last column of Table 2). We define *qlflag* = 0 for reliable sources (74.2% of the 200 M sample) and assign *qlflag* = 1 for those objects suspicious of suffering any potential problem (blending, contamination or non-stellar identification; 25.8% of the sample). As expected, the uncertainties in the RGB synthetic magnitudes are larger for the *qlflag* = 1 sources as displayed in Fig. 14.

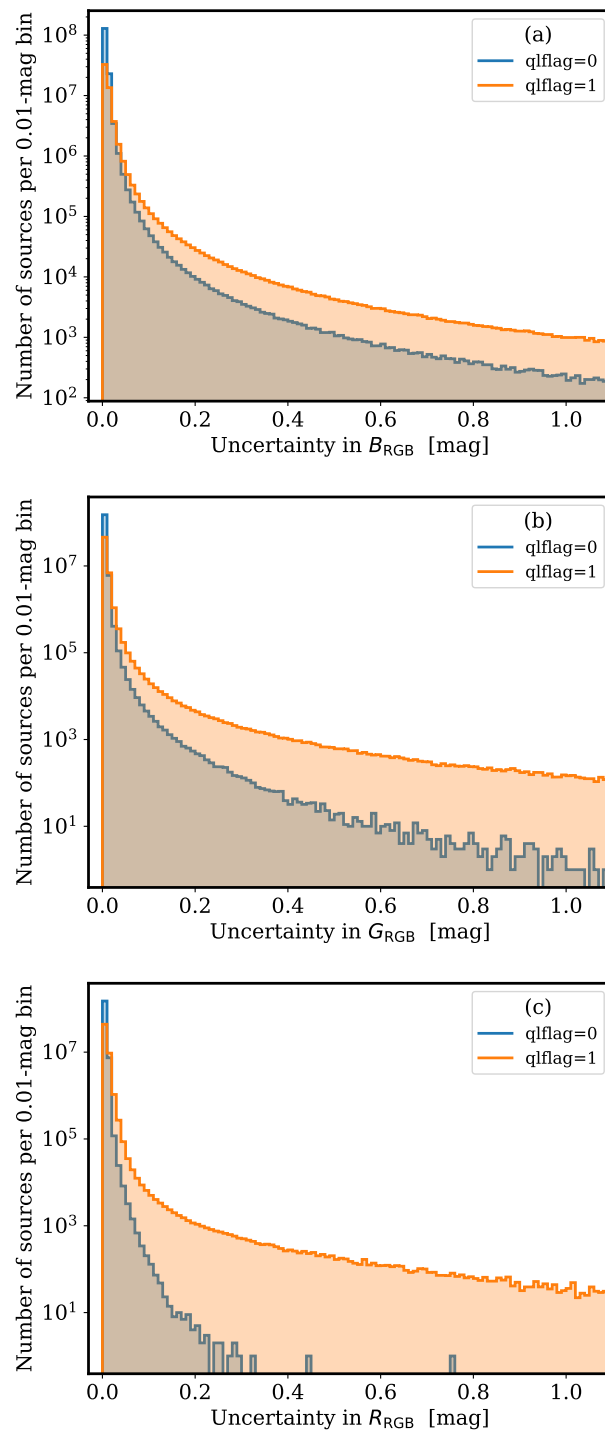


Figure 14. Histograms displaying the differences in the predicted uncertainties in the RGB synthetic magnitudes (panels (a), (b) and (c) for B_{RGB} , G_{RGB} and R_{RGB} , respectively) as a function of the global quality parameter $qlflag$ (last column in Table 2). As expected, the objects with poorer quality ($qlflag = 1$) exhibit larger uncertainties.

Complementary to the online table, in order to ease access to synthetic RGB photometry, we created a Python package called RGBLOOM (available at <https://github.com/guaix-ucm/rgbloom>, accessed on 24 March 2023), which performs cone search queries around any position

on the celestial sphere. This code is an updated version of RGBLUES (available at <https://github.com/guaix-ucm/rdblues>, accessed on 24 March 2023), the tool created by C21 to retrieve RGB magnitudes from the 15 M sample.

Once installed, the code can be easily executed from the command line—for example, using a command like this one:

```
$ rgbloom 56.66 24.10 1.0 12
```

The four numerical arguments correspond to the position search values (RA, DEC and search radius) in decimal degrees and the limiting G_{Gaia} magnitude. In the example command shown here, we are searching for sources brighter than $G_{\text{Gaia}} = 12$ mag within a circular aperture of radius 1 degree with centre at right ascension RA = 56.66 deg and declination DEC = 24.10 deg (corresponding to the Pleiades star cluster).

The steps followed by RGBLOOM to provide its output are the following:

1. Cone search in *Gaia* DR3 down to the pre-defined limiting G_{Gaia} magnitude, retrieving the following parameters: `source_id`, `ra`, `dec`, `phot_g_mean_mag`, `phot_bp_mean_mag`, `phot_rp_mean_mag` and `phot_variable_flag`.
2. Initial RGB magnitude estimation using the polynomial transformations given in Equations (2)–(4) by C21.
3. Retrieval of the RGB synthetic magnitudes for sources in the 200 M sample within the HEALPIX level-8 tables enclosing the region of the sky defined in the initial cone search.
4. Cross-matching between the *Gaia* DR3 and the 200 M subsamples to identify sources with RGB synthetic magnitudes estimated from the XP low-resolution spectra.
5. Generation of the output files. In particular, two files (in CSV format) are generated: `rgbloom_200m.csv`, which contains the sources belonging to the 200 M sample with RGB synthetic magnitudes; and `rgbloom_no200m.csv`, which includes sources that do not belong to the 200 M sample. In this latter case, the RGB magnitudes provided in the file correspond to the estimates derived using the polynomial relationships in C21. It is important to remember (see Section 3) that these estimates are more uncertain than the new RGB values computed in this work and that they can be biased due to systematic effects introduced by interstellar extinction by exhibiting a colour outside the $-0.5 \leq G_{\text{BP}} - G_{\text{RP}} \leq 2.0$ interval (where the C21 calibrations were computed) or by variability of the source.
6. Creation of a finding chart of the results (see the example in Figure 15 for the region around the Pleiades star cluster). The users of RGBLOOM should rely more strongly on the RGB estimates corresponding to sources belonging to the 200 M sample (labelled with red numbers in Figure 15) and make judicious use of the predictions that rely on the C21 polynomial calibration (labelled with black numbers in the same figure) as discussed in Section 4. Nevertheless, since the sky coverage of the 200 M sample is still not very good at certain high Galactic latitudes (see Figure 4), the RGB estimates from the C21 polynomial calibration may still be useful after discarding the sources with large interstellar extinction.

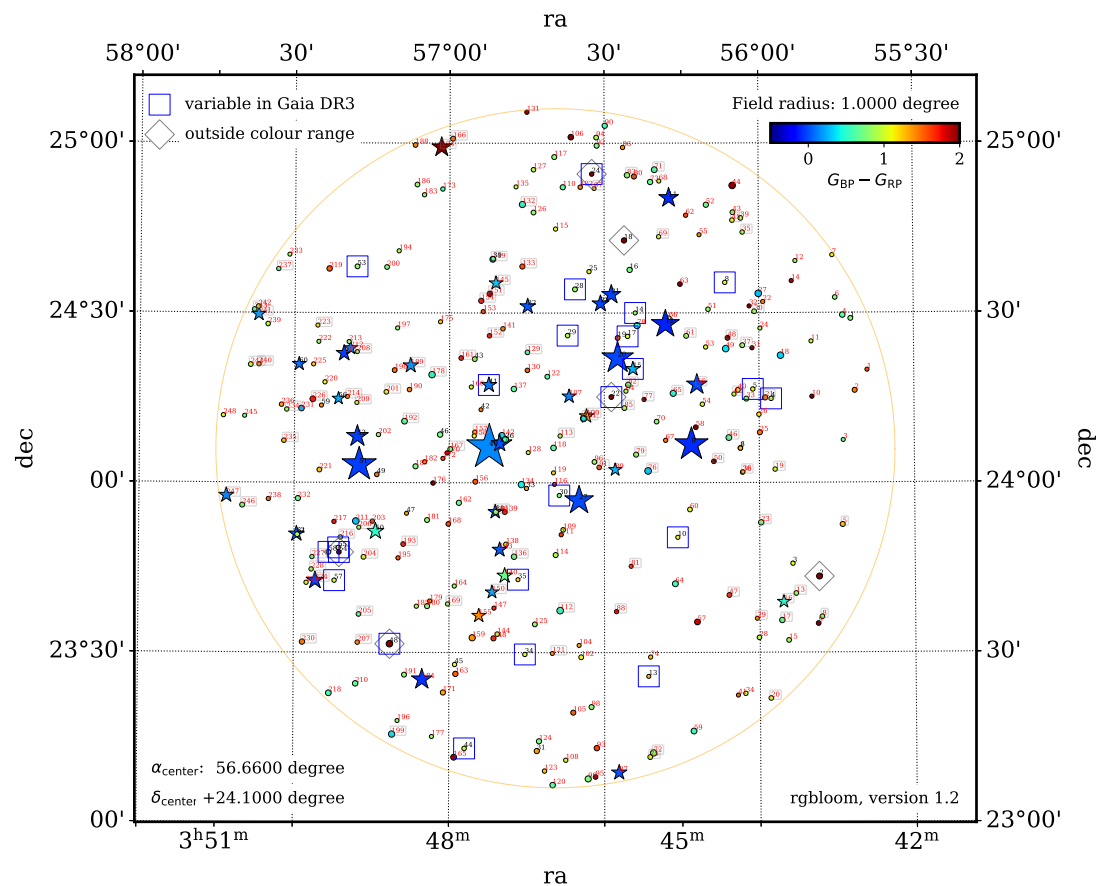


Figure 15. Example of a finding chart generated by the Python package RGBLOOM after performing a cone search centred in the Pleiades star cluster with a search radius of 1 degree. The objects in this plot are colour coded based on the *Gaia* $G_{BP} - G_{RP}$ colour and are numbered with labels of different colours (red or black for objects belonging or not to the 200 M sample, respectively) with numbers matching the first column of the output files `rgblloom_200m.csv` and `rgblloom_no200m.csv` generated during the execution of the code. The identification number of the less reliable sources in `rgblloom_200m.csv` (those with `qlflag=1`) appear within a rectangle with a light-gray colour. For sources that do not belong to the 200 M sample, and where RGB estimates correspond to the polynomial transformations from C21, which can be affected by systematic biases, the program overplots a blue square when the *Gaia* DR3 `phot_variable_flag` is set to VARIABLE and a grey diamond when the source colour is outside the $-0.5 \leq G_{BP} - G_{RP} \leq 2.0$ mag interval.

6. Conclusions

We provided, in this work, synthetic photometry in RGB passbands derived from *Gaia* DR3 XP spectrophotometry. The RGB magnitudes derived in this work represent a significant improvement over those published by C21 as they were directly derived from space-based SED observations and not predicted through photometric relationships as in C21. Although it is true that the *Gaia* XP spectra are of low spectral resolution by astrophysical standards, they constitute a clear improvement over the predictions obtained by the *Gaia* EDR3 G_{Gaia} , G_{BP} and G_{RP} integrated photometry employed by C21 to derive their polynomial calibration.

In addition, the new RGB estimates were derived employing the *Gaia* DR3 XP spectra, directly using their XP coefficients and their associated basis functions, which allows for preservation of the maximum information contained in the *Gaia* spectra as well as confident estimation of the propagation of uncertainties in the derived results. The number of calibrated

sources increased significantly, passing from ~ 15 million sources in C21 to slightly more than 200 million in this work. The new 200 M sample can now include sources without extinction restrictions and does not rely on any approximate calibration only valid for isolated solar metallicity stars.

In addition, the RGB magnitude estimates are provided with their associated uncertainties, which, in the C21 sample, were roughly estimated to be within a ± 0.1 mag interval and are now more robustly determined. In addition, the uncertainties for a considerable number of sources were within ± 0.01 mag, which constitutes a significant improvement. This means that, contrary to what happened with the C21 sample, whose RGB estimates should not be considered to be extremely accurate on a star-by-star basis, the availability of reliable uncertainties in the new 200 M catalogue allows us to infer quality photometric calibration even with a very small number of reference sources.

This work demonstrates that RGB photometry can already be performed using a vast catalogue of reliable calibration sources, available in a wide range of magnitudes and for a significant fraction of the celestial sphere. The astronomical magnitudes can easily be transformed into radiometric units by using the formulas published in [23].

Author Contributions: Conceptualization, J.M.C., A.S.d.M., J.Z. and N.C.; Computation J.M.C., N.C., S.P. and R.G.; Data analysis on the NightUp database J.M.C., N.C., S.P. and R.G.; Field test A.S.d.M., J.I., J.Z., J.M.C. and E.M. All authors have read and agreed to the published version of the manuscript.

Acknowledgments: This work was (partially) funded by the Spanish MICIN/AEI/10.13039/501100011033 and by “ERDF A way of making Europe” by the European Union through grants RTI2018-095076-B-C21 and PID2021-122842OB-C21 and the Institute of Cosmos Sciences University of Barcelona (ICCUB, Unidad de Excelencia ‘María de Maeztu’) through grant CEX2019-000918-M. Funding for the DPAC has been provided by national institutions—in particular, the institutions participating in the *Gaia* Multilateral Agreement. This project received funding from the European Union’s Horizon 2020 research and innovation programme under the Marie Skłodowska-Curie grant agreement No 847635 (UNA4CAREER). RALAN map project. This work made use of data from the European Space Agency (ESA) mission *Gaia* (<https://www.cosmos.esa.int/gaia>, accessed on 12 July 2022) processed by the *Gaia* Data Processing and Analysis Consortium (DPAC, <https://www.cosmos.esa.int/web/gaia/dpac/consortium>, accessed on 12 July 2022). This work was possible thanks to the extensive use of IPython and Jupyter notebooks [24]. This research made use of ASTROPY (<http://www.astropy.org>, accessed on 24 March 2023), a community-developed core Python package for Astronomy [25,26], NUMPY [27], SCIPY [28], MATPLOTLIB [29], PANDAS [30] and VAEX [31]. Some of the results in this paper were derived using the healpy and HEALPix packages [32,33].

Data Availability Statement: The BP/RP coefficients for all sources used here were obtained from the *Gaia* catalogue (<https://gea.esac.esa.int/archive/>, accessed on 12 July 2022). From them, we derived the RGB synthetic photometry, which can be accessed by following the detailed instructions in Section 5.

Conflicts of Interest: A. Sánchez de Miguel discloses that he does consulting work sporadically for Savestars Consulting S.L. and is a member of the board of Cel Fosc. The authors are not aware of any affiliations, memberships, funding or financial holdings that might be perceived as affecting the objectivity of this article.

References

1. Cardiel, N.; Zamorano, J.; Bará, S.; Sánchez de Miguel, A.; Cabello, C.; Gallego, J.; García, L.; González, R.; Izquierdo, J.; Pascual, S.; et al. Synthetic RGB photometry of bright stars: Definition of the standard photometric system and UCM library of spectrophotometric spectra. *Mon. Not. R. Astron. Soc.* **2021**, *504*, 3730–3748. <https://doi.org/10.1093/mnras/stab997>.
2. Cardiel, N.; Zamorano, J.; Carrasco, J.M.; Masana, E.; Bará, S.; González, R.; Izquierdo, J.; Pascual, S.; Sánchez de Miguel, A. RGB photometric calibration of 15 million *Gaia* stars. *Mon. Not. R. Astron. Soc.* **2021**, *507*, 318–329. <https://doi.org/10.1093/mnras/stab2124>.

3. Sánchez de Miguel, A.; Zamorano, J.; Aubé, M.; Bennie, J.; Gallego, J.; Ocana, F.; Pettit, D.R.; Stefanov, W.L.; Gaston, K.J. Colour remote sensing of the impact of artificial light at night (II): Calibration of DSLR-based images from the International Space Station. *Remote Sens. Environ.* **2021**, *264*, 112611.
4. Fulbright, J.P.; Xiong, X. Suomi-NPP VIIRS day/night band calibration with stars. In *Earth Observing Systems XX*; SPIE: San Diego, CA, USA, 2015; Volume 9607, pp. 488–508.
5. Wilson, T.; Xiong, X. Intercomparison of the SNPP and NOAA-20 VIIRS DNB high-gain stage using observations of bright stars. *IEEE Trans. Geosci. Remote Sens.* **2020**, *58*, 8038–8045.
6. Jiang, J.; Liu, D.; Gu, J.; Süssstrunk, S. What is the space of spectral sensitivity functions for digital color cameras? In Proceedings of the 2013 IEEE Workshop on Applications of Computer Vision (WACV), Clearwater Beach, FL, USA, 15–17 January 2013, pp. 168–179. <https://doi.org/10.1109/WACV.2013.6475015>.
7. Hoffleit, D. *Catalogue of Bright Stars*; Yale University Observatory: New Haven, CT, USA, 1964.
8. Gaia Collaboration; Brown, A.G.A.; Vallenari, A.; Prusti, T.; de Bruijne, J.H.J.; Babusiaux, C.; Biermann, M.; Creevey, O.L.; Evans, D.W.; Eyer, L.; et al. Gaia Early Data Release 3. Summary of the contents and survey properties. *Astron. Astrophys.* **2021**, *649*, A1, <https://doi.org/10.1051/0004-6361/202039657>.
9. Riello, M.; De Angeli, F.; Evans, D.W.; Montegriffo, P.; Carrasco, J.M.; Busso, G.; Palaversa, L.; Burgess, P.W.; Diener, C.; Davidson, M.; et al. Gaia Early Data Release 3. Photometric content and validation. *Astron. Astrophys.* **2021**, *649*, A3, <https://doi.org/10.1051/0004-6361/202039587>.
10. Carrasco, J.M.; Weiler, M.; Jordi, C.; Fabricius, C.; De Angeli, F.; Evans, D.W.; van Leeuwen, F.; Riello, M.; Montegriffo, P. Internal calibration of Gaia BP/RP low-resolution spectra. *Astron. Astrophys.* **2021**, *652*, A86. <https://doi.org/10.1051/0004-6361/202141249>.
11. De Angeli, F.; Weiler, M.; Montegriffo, P.; Evans, D.W.; Riello, M.; Andrae, R.; Carrasco, J.M.; Busso, G.; Burgess, P.W.; Cacciari, C.; et al. Gaia Data Release 3: Processing and validation of BP/RP low-resolution spectral data. *arXiv* **2022**. arXiv:2206.06143. .
12. Montegriffo, P.; De Angeli, F.; Andrae, R.; Riello, M.; Pancino, E.; Sanna, N.; Bellazzini, M.; Evans, D.W.; Carrasco, J.M.; Sordo, R.; et al. Gaia Data Release 3: External calibration of BP/RP low-resolution spectroscopic data. *arXiv* **2022**. arXiv:2206.06205. .
13. Gaia Collaboration; Vallenari, A.; Brown, A.; Prusti, T.e.a. Gaia Data Release 3: Summary of the content and survey properties. *arXiv* **2022**, *in press*.
14. Gaia Collaboration; Montegriffo, P.; Bellazzini, M.; De Angeli, F.; Andrae, R.; Barstow, M.A.; Bossini, D.; Bragaglia, A.; Burgess, P.W.; Cacciari, C.; et al. Gaia Data Release 3: The Galaxy in your preferred colours. Synthetic photometry from Gaia low-resolution spectra. *arXiv* **2022**. arXiv:2206.06215. .
15. Gaia Collaboration; Prusti, T.; de Bruijne, J.H.J.; Brown, A.G.A.; Vallenari, A.; Babusiaux, C.; Bailer-Jones, C.A.L.; Bastian, U.; Biermann, M.; Evans, D.W.; et al. The Gaia mission. *Astron. Astrophys.* **2016**, *595*, A1. . <https://doi.org/10.1051/0004-6361/201629272>.
16. Weiler, M.; Carrasco, J.M.; Fabricius, C.; Jordi, C. Analysing spectral lines in Gaia low-resolution spectra. *Astron. Astrophys.* **2023**, *671*, A52. <https://doi.org/10.1051/0004-6361/202244764>.
17. Carrasco, J.M.; Weiler, M.; Jordi, C.; Fabricius, C. Gaia, an all-sky survey for standard photometry. In *Highlights on Spanish Astrophysics IX*; Arribas, S., Alonso-Herrero, A., Figueras, F., Hernández-Monteagudo, C., Sánchez-Lavega, A., Pérez-Hoyos, S., Eds.; Spanish Astronomical Society 2017; pp. 622–627.
18. Weiler, M.; Carrasco, J.M.; Fabricius, C.; Jordi, C. Spectrophotometric calibration of low-resolution spectra. *Astron. Astrophys.* **2020**, *637*, A85. . <https://doi.org/10.1051/0004-6361/201936908>.
19. Fukugita, M.; Ichikawa, T.; Gunn, J.E.; Doi, M.; Shimasaku, K.; Schneider, D.P. The Sloan Digital Sky Survey Photometric System. *Astron. J.* **1996**, *111*, 1748. <https://doi.org/10.1086/117915>.
20. Bessell, M.S. Standard Photometric Systems. *Annu. Rev. Astron. Astrophys.* **2005**, *43*, 293–336. <https://doi.org/10.1146/annurev.astro.41.082801.100251>.
21. Sirianni, M.; Jee, M.J.; Benítez, N.; Blakeslee, J.P.; Martel, A.R.; Meurer, G.; Clampin, M.; De Marchi, G.; Ford, H.C.; Gilliland, R.; et al. The Photometric Performance and Calibration of the Hubble Space Telescope Advanced Camera for Surveys. *Publ. Astron. Soc. Pac.* **2005**, *117*, 1049–1112. . <https://doi.org/10.1086/444553>.
22. Crowley, C.; Kohley, R.; Hambly, N.C.; Davidson, M.; Abreu, A.; van Leeuwen, F.; Fabricius, C.; Seabroke, G.; de Bruijne, J.H.J.; Short, A.; et al. Gaia Data Release 1. On-orbit performance of the Gaia CCDs at L2. *Astron. Astrophys.* **2016**, *595*, A6. . <https://doi.org/10.1051/0004-6361/201628990>.
23. Sánchez de Miguel, A.; Aubé, M.; Zamorano, J.; Kocifaj, M.; Roby, J.; Tapia, C. Sky Quality Meter measurements in a colour-changing world. *Mon. Not. R. Astron. Soc.* **2017**, *467*, 2966–2979.
24. Pérez, F.; Granger, B.E. IPython: A System for Interactive Scientific Computing. *Comput. Sci. Eng.* **2007**, *9*, 21–29. <https://doi.org/10.1109/MCSE.2007.53>.
25. Astropy Collaboration; Robitaille, T.P.; Tollerud, E.J.; Greenfield, P.; Droettboom, M.; Bray, E.; Aldcroft, T.; Davis, M.; Ginsburg, A.; Price-Whelan, A.M.; et al. Astropy: A community Python package for astronomy. *Astron. Astrophys.* **2013**, *558*, A33. . <https://doi.org/10.1051/0004-6361/201322068>.

26. Astropy Collaboration; Price-Whelan, A.M.; Sipőcz, B.M.; Günther, H.M.; Lim, P.L.; Crawford, S.M.; Conseil, S.; Shupe, D.L.; Craig, M.W.; Dencheva, N.; et al. The Astropy Project: Building an Open-science Project and Status of the v2.0 Core Package. *Astron. J.* **2018**, *156*, 123. . <https://doi.org/10.3847/1538-3881/aabc4f>.
27. Harris, C.R.; Millman, K.J.; van der Walt, S.J.; Gommers, R.; Virtanen, P.; Cournapeau, D.; Wieser, E.; Taylor, J.; Berg, S.; Smith, N.J.; et al. Array programming with NumPy. *Nature* **2020**, *585*, 357–362. <https://doi.org/10.1038/s41586-020-2649-2>.
28. Virtanen, P.; Gommers, R.; Oliphant, T.E.; Haberland, M.; Reddy, T.; Cournapeau, D.; Burovski, E.; Peterson, P.; Weckesser, W.; Bright, J.; et al. SciPy 1.0: Fundamental Algorithms for Scientific Computing in Python. *Nat. Methods* **2020**, *17*, 261–272. <https://doi.org/10.1038/s41592-019-0686-2>.
29. Hunter, J.D. Matplotlib: A 2D Graphics Environment. *Comput. Sci. Eng.* **2007**, *9*, 90–95.
30. Wes McKinney. Data Structures for Statistical Computing in Python. In Proceedings of the ninth Python in Science Conference, Austin, TX, USA, 28 June–3 July 2010; Stéfan van der Walt.; Millman, J., Eds.; pp. 56–61. <https://doi.org/10.25080/Majora-92bf1922-00a>.
31. Breddels, M.A.; Veljanoski, J. Vaex: Big data exploration in the era of Gaia. *Astron. Astrophys.* **2018**, *618*, A13. . <https://doi.org/10.1051/0004-6361/201732493>.
32. Górski, K.M.; Hivon, E.; Banday, A.J.; Wandelt, B.D.; Hansen, F.K.; Reinecke, M.; Bartelmann, M. HEALPix: A Framework for High-Resolution Discretization and Fast Analysis of Data Distributed on the Sphere. *Astrophys. J.* **2005**, *622*, 759–771. . <https://doi.org/10.1086/427976>.
33. Zonca, A.; Singer, L.; Lenz, D.; Reinecke, M.; Rosset, C.; Hivon, E.; Gorski, K. healpy: Equal area pixelization and spherical harmonics transforms for data on the sphere in Python. *J. Open Source Softw.* **2019**, *4*, 1298. <https://doi.org/10.21105/joss.01298>.